ICY SATELLITE AND LUNAR EJECTA FROM MAPPING OF SECONDARY CRATERS: IMPLICATIONS FOR SESQUINARY FORMING FRAGMENTS. Kelsi N. Singer[1], William B. McKinnon[2], Bradley L. Joliff[2], Jeffery B. Plescia[3]. [1]Southwest Research Institute, 1050 Walnut Street, Boulder, CO 80302, United States (ksinger@boulder.swri.edu). [2]Department of Earth and Planetary Sciences, Washington University in St. Louis, MO 63130. [3]Applied Physics Laboratory, MS 200-W230, 11000 Johns Hopkins Road, Laurel, MD 20723.

Introduction: Observations are necessary to validate experiments and modeling of cratering and ejecta physics. We have mapped six secondary crater fields on the Moon, two on Ganymede, and one on Europa. We applied crater scaling laws to estimate the size and velocity of the ejecta fragments that formed each secondary. We characterize two main aspects of the data: 1) the secondary size fall-off as a function of distance from the primary crater (discussed elsewhere [1]), and 2) the size-velocity distribution (SVD) of ejected fragments (the focus of this abstract). These data can be compared for craters across the Solar System—on the Moon [1-3], terrestrial planets [2,3], icy satellites [4], and small bodies—to examine trends and assess the role of material and dynamical parameters in fragment formation and ejection.

We find an unexpected scale-dependent trend in ejecta fragment SVDs and empirically estimate the maximum fragment sizes reaching escape velocity.

Mapping: With the Lunar Reconnaissance Orbiter (LRO) dataset we can explore a range of primary crater sizes. The LRO Wide Angle Camera (WAC) 100 m px^{-1} global mosaic served as the base for all mapping. We also examined Narrow Angle Camera (NAC) images (~0.5–1.5 m px^{-1}) for confirmation of secondary crater morphologies. Both Galileo and Voyager 2 images were used in the mapping of Europa and Ganymede [details in 4]. Only the craters with the highest likelihood of being secondaries (in obvious radial chains or clusters), and whose diameters were clear, are used in the subsequent analysis. A summary of mapped locations is given in Table 1.

Ejecta Fragment Size-velocity Distributions (SVDs): We estimated the velocity (v_{ej}) and size (d_{frag}) of the ejecta fragment that formed each secondary crater from the range equation for a ballistic trajectory on a sphere [7] and Schmidt-Holsapple scaling relations (methods as in [5]). Size scaling was carried out with the full equations spanning the gravity and strength regime and for both non-porous and porous endmember target material properties [e.g., refs. 8,9]. Primary crater transient cavity diameters were estimated according to [10,11].

A power law function was fit to the upper envelope (99th quantile) of the SVDs using quantile regression [12]: $d_{frag,max} = \alpha v_{ej}^{-\beta}$ (shown in Fig. 1 for Copernicus). The upper envelope provides the maximum secondary crater size, assuming all smaller sizes are possible down to the resolution limit (confirmed by inspection).

Results and Discussion: As expected, the fragment magnitude factor, α, generally scales with primary crater size. Icy satellite secondary crater magnitudes (a) follow a similar trend to, but are lower values than the lunar examples. Current spallation theory

Table 1 – Primary crater and secondary field characteristics.

Primary Crater	Final Primary Diameter (km)[a]	Primary Transient Diameter (km)[b]	Primary Impactor Diameter (km)	Number of Secondaries Mapped	Largest Observed Secondary (km)[b]	Average of Largest 5 Secondaries (km)[b]	Estimated Max Fragment Size at Escape Velocity (m)[c]
Orientale	660	360	85	245	26 (4%)	23 (4%)	860 (4700)
Copernicus	93	63	9.3	4,565	5.5 (6%)	4.9 (5%)	50 (380)
Kepler	31	24	2.7	1,200	1.4 (5%)	1.3 (4%)	40 (300)
Unnamed in SPA	3.0	2.5	0.16	2,000	0.18 (5%)	0.16 (5%)	3 (30)
Unnamed near Orientale	2.2	1.8	0.11	2,645	0.10 (5%)	0.08 (4%)	5 (50)
Unnamed in Procellarum	0.83	0.68	0.038	1,730	0.04 (5%)	0.04 (5%)	5 (50)
Icy Satellites:							
Gilgamesh (G)	585	271	49	445	21 (4%)	-	220 (1600)
Tyre (E)	38	23	1.8	1,165	2.8 (7%)	-	120 (900)
Achelous (G)	35	21	1.9	630	2.7 (8%)	-	36 (400)

[a]Final diameter for Orientale is estimated at the Outer Rook Mountains, and for Gilgamesh and Tyre based scaling from ejecta deposits to rim locations for other large craters on icy bodies [5,6]. [b]Percentage of primary crater size given in parentheses. [c]Hill sphere escape velocity used: 2.34, 2.63, and 1.91 km s^{-1} for the Moon, Ganymede, and Europa, respectively. Sesquinary crater size for re-impact on the same body is given in parentheses - for typical re-impact speeds [4,17,18], for the Moon, re-impact speeds vary depending on dynamical fate [20], above given for 3 km s^{-1} for reference. Note these fragments would not necessarily stay intact.

[7,13] predicts $\beta = 1$, and β is limited to the interval {1,4/3} by coupling parameter scaling in the gravity regime for the specific case when $d_{frag,max}$ does not depend on the target sounds speed (see [4], App. C). The β parameter is observed, however, to vary between 0.2 and 3 on both icy and rocky bodies [3,14,15].

This large range of β could mean a more complicated scaling applies than derived in Singer et al. [4]. Otherwise, this range of β indicates the material response to the passage of the shock wave is scale dependent. The shallow βs found for the smaller primaries imply a weaker dependence on material strength (nominally, tensile strength for spallation) than is exhibited by the larger craters with steeper β values [ref. 4, Eqn A.20]. For the smaller primary craters, we may be seeing the influence of a fundamental block size (pre-existing fractures/layering in the target), however, the block sizes still scale with primary size even for the smallest primaries. This scale dependence may be related to the velocity dependence seen in recent numerical simulations [16].

Largest Fragments at Escape Velocity: Extrapolating the power-law fits for largest fragment size to the Hill-sphere escape velocity for each body yields escape fragment sizes for the Moon of a few meters for the smaller primary craters (D < 3 km), a few 10s of meters for mid-sized primary craters (D = 30–100 km), and up to ~900 m for the Orientale basin (Table 1). At these high velocities, however, and given the fractured nature of the lunar regolith or mega-regolith, the material would likely break up in flight.

Escaped fragments would go into orbit, and may eventually re-impact the parent body, or impact a nearby moon or planet, potentially forming a so-called sesquinary crater. A particular ejecta fragment's dynamical evolution would depend on its launch position (latitude and longitude), ejection angle, and ejection velocity [17-21]. A small percentage of the lunar fragments may end up in the meteorite collection.

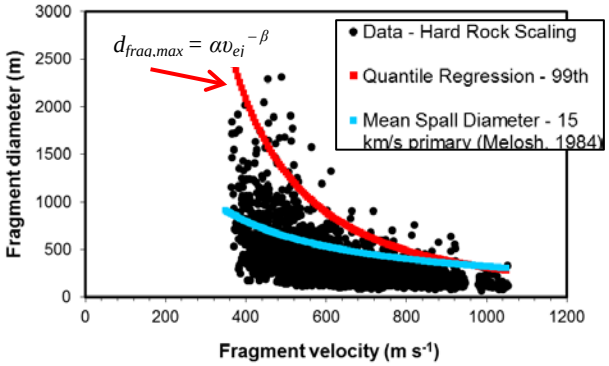

Figure 1. Estimated fragment sizes for forming Copernicus' secondary craters, quantile regression fit to upper envelope, and estimated mean spall diameter for a primary projectile impacting the Moon at 15 km s^{-1} [7,13].

Acknowledgement: NASA, PG&G, NESSF, LRO, and the LROC Team for images and funding to carry out this work.

References: [1] Singer K.N. et al. (2104) *LPSC abs*. #1162. [2] Vickery A.M. (1986) *Icarus 67*, 224-236. [3] Vickery A.M. (1987) *GRL 14*, 726-729. [4] Singer K.N. et al. (2103) *Icarus 226*, 865-884. [5] Schenk P. M. and Ridolfi F. J. (2002) *GRL 29*, 31-1. [6] Schenk P. M. and Turtle, E. (2009) In Europa. UAP, Tucson, pp. 181-198. [7] Melosh H.J. (1989) Impact Cratering: A Geologic Process. OUP, p. 107. [8] Holsapple K.A. (1993) *AREPS 21*, 333-373. [9] Holsapple K.A. (2007) http://keith.aa.washington.edu/crater-data/scaling/theory.pdf. [10] McKinnon W.B. and Schenk P.M. (1985) *LPSC XVI*, 544-545. [11] McKinnon W.B. and Schenk P.M. (1995) *GRL 22*, 1829-1832. [12] Koenker R. (2005) Quantile Regression. CUP, New York. [13] Melosh H.J. (1984) *Icarus 59*, 234-260. [14] Hirata N. and Nakamura A. M. (2006) *JGR 111*, E03005. [15] Hirase Y. et al. (2004) *P&SS 52*, 1103-1108. [16] Johnson B.C. and Melosh H.J. (2014) *Icarus 228*, 347-363. [17] Alvarellos J.L. et al. (2002) *Icarus 160*, 108-123. [18] Alvarellos J.L. et al. (2005) *Icarus 178*, 104-123. [19] Zahnle et al. (2008) Icarus 194, 660-674. [20] Gladman B. et al. (1995) *Icarus 118*, 302-321. [21] Kreslavsky M.A. and Asphaug E. (2014) *LPSC abs*. #1162.

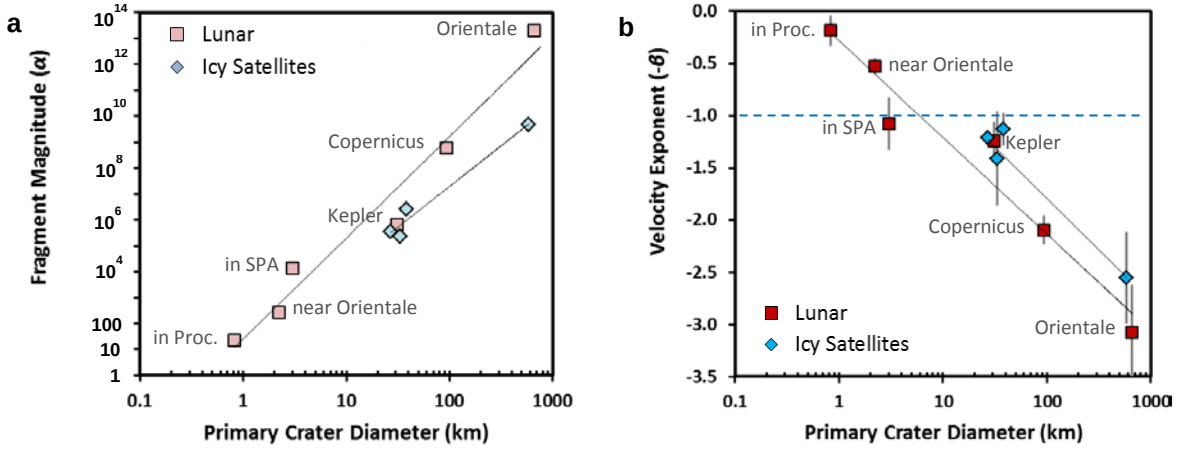

Figure 2. Quantile regression parameters α and $-\beta$ for the upper envelope (99th quantile) of each ejecta fragment size-velocity distribution (example in Fig. 1). The velocity exponent predicted by spallation theory [7,13], $-\beta = -1$, is highlighted for reference in **b**.